isvr Institute of Sound and Vibration Research

A Report on the Development of an Algorithm that Incorporates Depth Dependence in the Dispersion Relation for Bubbly Media

T.G. Leighton, M.D. Simpson, J.W.L. Clarke and S.D. Meers

ISVR Technical Report No 290

November 2000

University of Southampton

SCIENTIFIC PUBLICATIONS BY THE ISVR

Technical Reports are published to promote timely dissemination of research results by ISVR personnel. This medium permits more detailed presentation than is usually acceptable for scientific journals. Responsibility for both the content and any opinions expressed rests entirely with the author(s).

Technical Memoranda are produced to enable the early or preliminary release of information by ISVR personnel where such release is deemed to the appropriate. Information contained in these memoranda may be incomplete, or form part of a continuing programme; this should be borne in mind when using or quoting from these documents.

Contract Reports are produced to record the results of scientific work carried out for sponsors, under contract. The ISVR treats these reports as confidential to sponsors and does not make them available for general circulation. Individual sponsors may, however, authorize subsequent release of the material.

UNIVERSITY OF SOUTHAMPTON
INSTITUTE OF SOUND AND VIBRATION RESEARCH
FLUID DYNAMICS AND ACOUSTICS GROUP

A Report on the Development of an Algorithm that Incorporates Depth Dependence in the Dispersion Relation for Bubbly Media

by

T G Leighton, M D Simpson, J W L Clarke and S D Meers

ISVR Technical Report No. 290

November 2000

Authorized for issue by
Professor P A Nelson
Group Chairman

ACKNOWLEDGEMENTS

Professor Leighton is grateful to Simon Richards for assistance in the formulation of the problem, and to Professor Farmer for supplying unpublished data. This report was funded under agreement EA 1590 (Project 6183).

CONTENTS

LIST OF SYMBOLS

a_0	Empirical value used for the continuity of bubble density functions in the radius domain
A'	Scaling term in empirical expression
A''	Scaling term in empirical expression
B	Empirical value used for the continuity of bubble density functions
b	Damping constant of an oscillating bubble
c	Speed of acoustic waves in liquid
c_c	Complex sound speed of a bubbly liquid
c_f	Speed of sound in bubble-free water
D	Gas thermal diffusivity
D_e	E-folding depth (m)
e	Exponential constant, ≈ 2.718281828
f	Insonification frequency (Hz)
F	Insonification frequency (kHz)
F_{rb}	Relaxation frequency of Boric acid (kHz)
F_{rm}	Relaxation frequency of Magnesium sulphate (kHz)
g	Acceleration due to gravity (9.81 m/s^2)
h	Water height
I_p	Intensity of a plane wave measured at $x = 0$
I_x	Intensity of a plane wave measured at some distance x
j	$\sqrt{(-1)}$
k	Acoustic wave number
k_c	Complex acoustic wavenumber
K_c	Complex compressibility
K_v	Compressibility
$n_b(R_0)$	Bubble distribution: number of bubbles per micrometer radius
p	Total pressure
$p(R_0)$	Bubble density function
p_1	Exponent constant
p_2	Exponent constant
p_o	Hydrostatic pressure
P	Acoustic pressure (Pa)
P_p	Acoustic rms pressure at $x = 0$
P_x	Acoustic rms pressure at some distance x
q	The real part of the complex wave number
R_0	Equilibrium bubble radius (m)
S_{ppt}	Salinity (ppt)
t	Time (s)
T	Temperature (°C)
u	Real part of the phase speed ratio
v	Imaginary part of the phase speed ratio
V	Volume
V_d	Dispersive phase speed
W	Wind speed (m/s)
x	Distance co-ordinate
z	Water depth ($z = -h$)
α	Attenuation coefficient (dB/m)

α_e	Attenuation rate (Np/m)
α_f	Attenuation rate of pure water (Np/m)
α_s	Attenuation rate of sea water (Np/m)
γ	Ratio of specific heats at constant pressure to that at constant volume
π	Pi $\approx$ 3.14159
Φ	Thermal scaling factor
κ	Polytropic index of the gas inside the bubble
μ	Shear viscosity of fluid
μ_f	Shear viscosity of pure water
μ'_f	Bulk viscosity of pure water
σ	Surface tension coefficient
ρ	Density of the fluid surrounding the bubble
ρ_f	Density of pure water
ρ_S	Density of sea water
ω	Insonifying frequency (rad/s)
ω_i	Angular frequency of the imaging sound field (rad/s)
ω_o	Angular resonance frequency of the bubble (rad/s)
ω_p	Angular frequency of the pumping sound field (rad/s)
χ	Abbreviation term
$\Im$	Imaginary part of a complex number
$\Re$	Real part of a complex number
SPL	Sound Pressure Level
VF	Void fraction describing the bubble population

TABLE OF FIGURES

1.0 INTRODUCTION

This report will detail the development of a depth dependant algorithm for the calculation of phase speed and attenuation for a plane acoustic wave in a bubbly medium.

First, the physics of the dispersive properties of bubbly media will be described, culminating with appropriate equations for *depth independent* phase speed and attenuation.

Second, explanations of the variation of a bubble population with depth will be presented, resulting in the adaptation of existing dispersion algorithms to incorporate depth dependence.

This report will conclude with a summary of the equations required by the reader to perform meaningful simulations of the effect of depth dependent bubble populations on a ray-tracing model of the surface layer of the oceans.

2.0 DISPERSION CAUSED BY BUBBLES

A plane wave travelling through a bubbly liquid will be attenuated more than in a bubble-free liquid because of the added absorption and scattering effects of the bubbles. Bubbles also cause the compressibility of the fluid volume to be complex. Complex compressibility equates to a dispersive medium (Leighton, 1994).

Before detailing the physics of the propagation of a plane wave through a bubbly liquid, this chapter will start by presenting the calculations for the attenuation of a plane wave in a bubble-free environment, since it is the *excess* attenuation presented to a plane wave in a bubbly medium that is detailed later in this section.

2.1 Homogeneous Attenuation of a Plane Wave

When there are no scattering processes involved, a plane wave is attenuated by the conversion of acoustic energy into heat. Acoustic losses in sea water are caused by the effects of shear viscosity, bulk viscosity and relaxation processes. The attenuation of a plane wave is usually characterised by the *Attenuation Coefficient* and is measured in dB per meter (Clay and Medwin, 1977).

2.1.1 *The Attenuation Coefficient*

The rate of decrease of pressure amplitude (P) with distance (x) in a progressive plane wave is proportional to the pressure amplitude of the wave.

$$\frac{dP}{dx} = -(\alpha_e)P_p \tag{1}$$

Integrating with respect to x gives,

$$P_x = P_p \exp(-\alpha_e x) \tag{2}$$

where P_x is the rms pressure at some distance x, P_p is the rms pressure at $x = 0$ and α_e is the exponential pressure attenuation *rate* measured in units of Np/m (Nepers per metre).

The plane wave attenuation *coefficient* measured in decibels is proportional to the logarithm of the pressure ratio which can be found from equation (2), as follows:

$$dBloss = 20\log_{10}\left(\frac{P_p}{P_x}\right) = (\alpha_e)x(20\log_{10} e) = 8.686(\alpha_e)x \tag{3}$$

The attenuation coefficient, α (dB/m), is therefore expressed as,

$$\alpha = 8.686\alpha_e \tag{4}$$

Substituting equation (3), gives

$$dBloss = \alpha x \tag{5}$$

2.1.2 *Attenuation Coefficient of Sea Water*

The attenuation coefficient of a plane wave in pure water is dominated by the shear and bulk viscosities of the water and is proportional to the square of the frequency (figures 1a and 1b). To extend the pure water model to sea water, the relaxation processes of magnesium sulphate and boric acid are added to the pure water term. Shear viscosity losses are caused by the frictional forces due to the relative motion of adjacent layers of the liquid. Bulk viscosity is caused by molecular rearrangements that occur during a cycle of the sound wave. The time necessary to reorder the molecules of the medium in response to the changing pressure of the sound wave is termed the *relaxation time*. Acoustic losses due to relaxation processes depend upon the period of the sound wave and its relation to the relaxation time. Large losses are evident when the two times are comparable and small losses are evident when the two times are significantly different (Clay and Medwin, 1977).

The attenuation rate for fresh water is described in the following empirical expression (Clay and Medwin, 1977),

$$\alpha_f = \frac{4.34}{\rho_f c_f^3}\left(\frac{4\mu_f}{3} + \mu'_f\right)\omega^2 \quad \text{(dB/m)} \tag{6}$$

where ρ_f is the density of pure water, μ_f and μ_f' are the shear and bulk viscosity of water respectively and ω is the insonifying frequency in rad/s. Shear and bulk viscosities are temperature dependent. For the purpose of calculations, a temperature of 14°C was used, giving values of 1.2×10^{-3} Ns/m^2 for shear viscosity and 3.3×10^{-3} Ns/m^2 for the bulk viscosity of pure water.

The addition of the relaxation processes to equation (6) gives the empirical attenuation rate for sea water *(α_s)* (Clay and Medwin, 1977):

$$\alpha_s = \frac{1.71\times10^8\left(4\mu_f/3+\mu'_f\right)F^2}{\rho_f c_f^3}+\left(\frac{S_{ppt}A'F_{rm}F^2}{F^2+F_{rm}^2}\right)\left(1-1.23\times10^{-3}P_o\right)+\left(\frac{A''F_{rb}F^2}{F^2+F_{rb}^2}\right) \quad (7)$$

The salinity of the water, S_{ppt}, is in parts per thousand. The terms F_{rm} and F_{rb} are the temperature dependant relaxation frequencies of the magnesium sulphate and boric acid respectively in kHz. The insonification frequency, F, is expressed in kilohertz, A' and A'' are scaling factors that convert their respect terms in equation (7) to decibels per unit distance (Clay and Medwin, 1977). The hydrostatic head pressure, P_0, due to the water column given is by,

$$P_0 = \rho_s g h \quad (8)$$

The sound speed, c_f, in the bubble-free water is a function of temperature, depth and salinity. Several formulations exist, Clay and Medwin (1977) give the following empirical expression:

$$c_f = 1449.2+4.6T-0.055T^2+0.00029T^3+\left(1.34-0.010T\right)\left(S_{ppt}-35\right)+1.58\times10^{-6}P_o \quad (9)$$

where T (°C) is the water temperature.

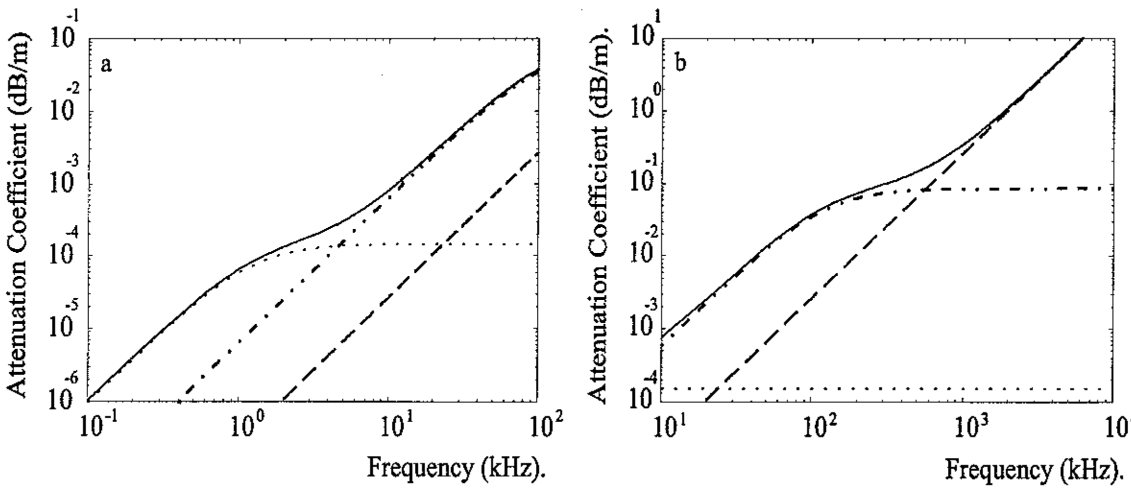

Figure 1: The attenuation coefficient due to absorption in sea water (solid line) at 16°C and salinity at 35 ppt with contributions from fresh water (large dashes) and relaxation contributions from boric acid (small dashes) and magnesium sulphate (dash-dot). a) Frequency window is 0.1 to 100 kHz. b) Frequency window is 10 to 10000 kHz.

2.2 The Dispersive Bubbly Medium

Since the bubble can be viewed as a single degree of freedom oscillator (Leighton, 1994), the driving force on the bubble delivered by the insonifying sound field will not always be in phase with volume changes of the bubble. Therefore, the compressibility (K_v) of a bubbly medium will be complex since compressibility is the ratio of the volume (V) to pressure (p) changes.

$$K_v = \left(\frac{-1}{V}\right)\left(\frac{dV}{dp}\right) \tag{10}$$

The complex compressibility of the bubbles can be added to the compressibility of the bubble free water of a bubbly medium. This gives rise to a complex phase speed given by equation (11).

$$c_c{}^2 = \left(K_c \rho\right)^{-1} = \left(\frac{\omega}{k_c}\right) \tag{11}$$

where K_c and k_c are the complex compressibility and wave number respectively.

The pressure given in equation (2) can be expressed as a progressive pressure wave travelling in the positive x-direction by,

$$P_x = P_p \exp j(\omega t - qx)\exp(-\alpha_e x) \tag{12}$$

In this form, it can be seen that the complex wave number takes the form $k = q + j\alpha_e$ since $\exp(jkx) = \exp(jqx)\exp(-\alpha x)$. The imaginary part of the complex wave number describes the attenuation whilst the real part describes the sound speed, (Leighton, 1994).

Commander and Prosperetti (1989) give the complex wave number for a bubbly liquid as,

$$k_c^2 = \frac{\omega^2}{c^2} + 4\pi\omega^2 \int_{R_0=0}^{\infty} \frac{R_0 n_b(R_0) dR_0}{\omega_0^2 - \omega^2 + 2jb\omega} \tag{13}$$

where R_0 is the equilibrium radius of the bubble and $n_b(R_0)dR_0$ is the number of bubbles having radii between R_0 and dR_0 in a unit volume of test fluid. The resonant frequency of the bubble is ω_0 (see section 4) and ω is the frequency of the insonifying sound field. It is traditional to set dR_0 to 1 μm which has the effect of summing the effect of number of bubbles, $n_b(R_0)$, over each micrometer bin. The damping constant b is a summation of the viscous, thermal and acoustic damping of the bubble. Commander and Prosperetti (1989) give the following expression for b:

$$b = \frac{2\mu}{\rho R_0{}^2} + \frac{p_0}{2\rho R_0{}^2 \omega}\Im\Phi + \frac{\omega^2 R_0}{2c} \tag{14}$$

The shear viscosity of the liquid is μ, p_0 is the equilibrium pressure in the bubble and Φ is a thermal scaling factor given by,

$$\Phi = \frac{3\gamma}{1-3(\gamma-1)j\chi\left[(j/\chi)^{1/2}\coth(j/\chi)^{1/2}-1\right]} \tag{15}$$

where,

$$\chi = \frac{D}{\omega R_0{}^2} \tag{16}$$

The gas thermal diffusivity is given by D and γ is the ratio of specific heat of the gas at constant pressure against that at constant volume.

The complex sound speed of the bubbly liquid is given by,

$$c_c = \frac{\omega}{k_c} \tag{17}$$

Therefore, equation (13) becomes,

$$\frac{c^2}{c_c^2} = 1 + 4\pi c^2 \int_{R_0=0}^{\infty} \frac{R_0 n_b(R_0)dR_0}{\omega_0^2 - \omega^2 + 2jb\omega} \tag{18}$$

Setting the square root of the above ratio to a real and imaginary part,

$$\frac{c}{c_m} = u - jv \tag{19}$$

the real part, u, is used to determine the phase speed through,

$$V_d = \frac{c}{u} \quad (\mathrm{ms}^{-1}) \tag{20}$$

and the imaginary part, v, determines the attenuation coefficient,

$$\alpha = 20(\log_{10} e)\left(\frac{\omega v}{c}\right) \quad (\mathrm{dB/m}) \tag{21}$$

Equations (20) and (21) allow the exact calculation of phase speed variations and excess attenuation with frequency for any given bubble population.

2.2.1 *Analysis of Model Bubble Populations*

As an initial test, a set of bubble population models were applied to the dispersion algorithms of equations (20) and (21) and the frequency-dependant phase speed and attenuation coefficients were calculated. Finally, the data collected from a sea trial in the Solent (Leighton *et al*, 1998), using the combination frequency technique, was also applied to determine the magnitude of effect on phase speed and attenuation presented by a typical oceanic bubble population.

a) A mono-disperse bubble population

Figures 2a and 2b show the phase speed and excess attenuation that was derived for a mono-disperse bubble population of equilibrium bubble radius of 0.994 mm and a void fraction[1] of 0.0377%. It should be noted that the global maximum in the attenuation plot occurs at the resonant frequency of the bubble population. The phase speed asymptotes to a bubble free phase speed at high insonification frequencies. Figures 2c and 2d plot the phase speed and attenuation for the same mono-disperse bubble size but with varying void fractions. It can be seen that the reduction in the number of bubbles reduces the phase speed and attenuation variation. The behaviour of phase speed and attenuation as a function of void fraction (figures 2c and 2d) should be noted as an indication of the behaviour of these two quantities with respect to depth since bubble populations are also a function of depth (as will be shown in section 3.2).

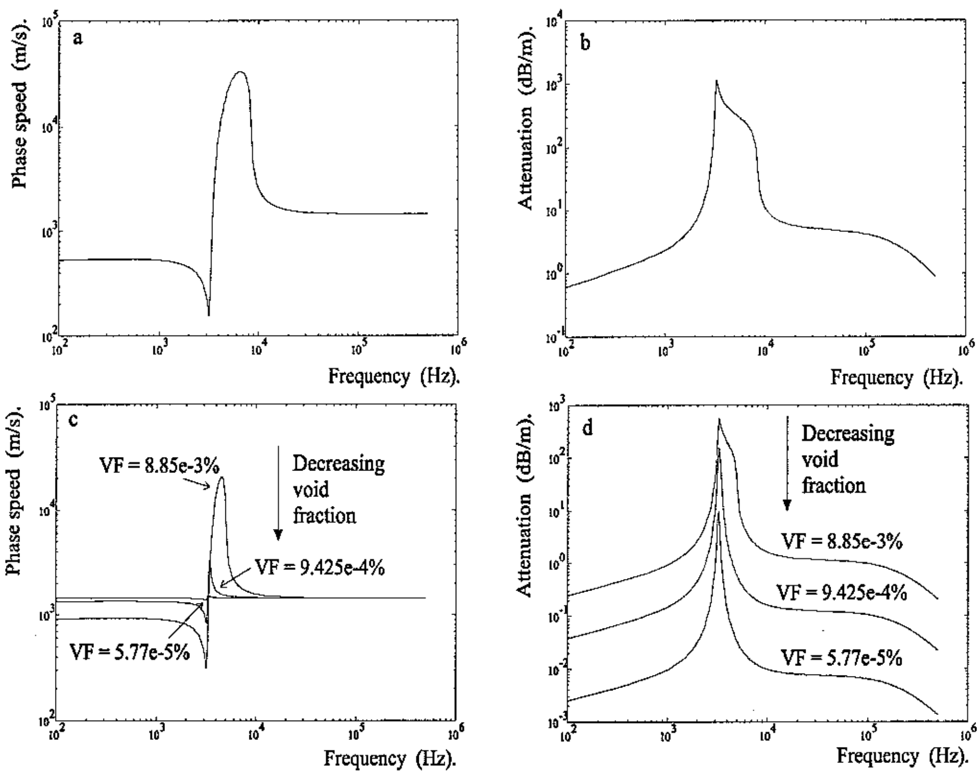

Figure 2: a) Phase speed of pressure waves incident on a mono-disperse bubble population of equilibrium radius 0.994 mm and a void fraction of 0.0377%. b) The excess attenuation evident of a pressure wave incident on a mono-disperse bubble population of equilibrium radius 0.994 mm and a void fraction of 0.0377%. c) Phase speeds of a pressure wave incident on mono-disperse bubble

[1] The Void Fraction (*VF*) is the percentage of gas in the liquid medium.

populations all of equilibrium radius 0.994 mm and decreasing void fractions. d) The excess attenuation evident of a pressure wave incident on a mono-disperse bubble population all of equilibrium radius 0.994 mm and a decreasing void fraction.

b) A bi-disperse bubble population

Figures 3a and 3b show the phase speed and excess attenuation that was derived for a bi-disperse bubble population consisting of two equilibrium radii of 1.13 and 2.53 mm with respective void fractions of 0.0421 and 0.0256%.

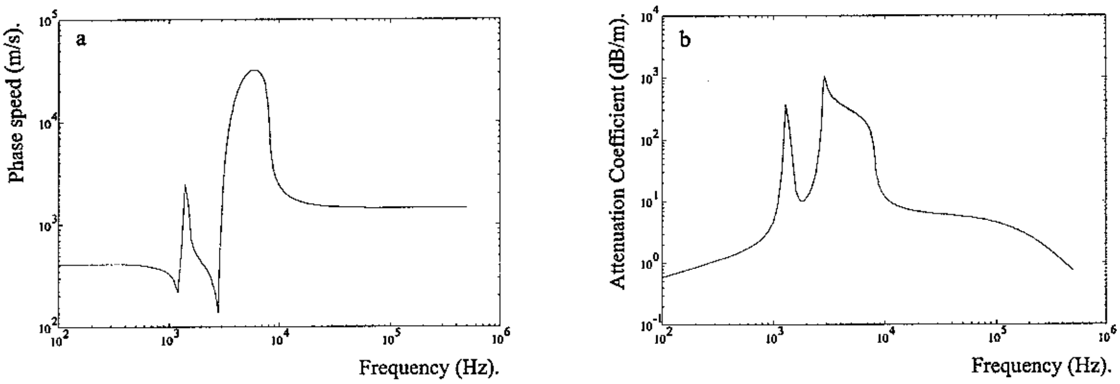

Figure 3: a) Phase speed of pressure waves incident on a bi-disperse bubble population consisting of two equilibrium radii of 1.13 and 2.53 mm with respective void fractions of 0.0421 and 0.0256%. b) The excess attenuation evident of pressure waves incident on a bi-disperse bubble population consisting of two equilibrium radii of 1.13 and 2.53 mm with respective void fractions of 0.0421 and 0.0256%.

c) A typical oceanic bubble population taken from the first sea trial using the combination frequency technique (Leighton et al, 1998)

Figure 4a shows a typical bubble population measured by the combination frequency technique during the first sea trial. This distribution was put into the dispersive phase speed and attenuation model (equations (20) and (21)) to produce figures 4b and 4c.

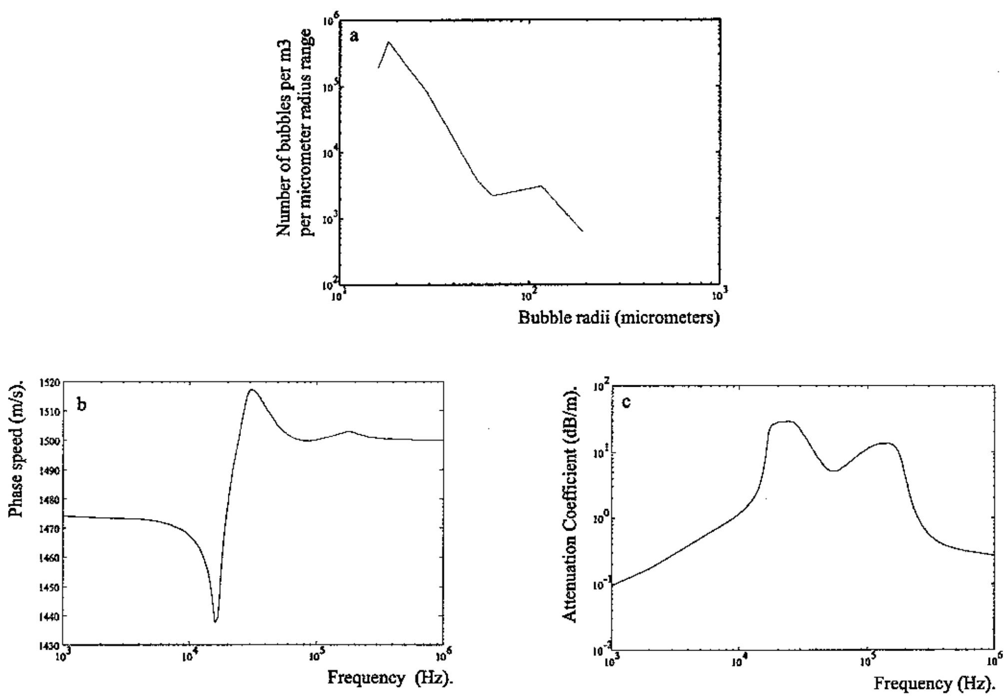

Figure 4: a) A bubble distribution function taken from a sea trial using the combination frequency technique. b) Phase speed variations with frequency derived for the bubble population shown in figure 4a. c) The excess attenuation with frequency derived for the bubble population shown in figure 4a.

3.0 THE DEPTH DEPENDENCE OF MODEL BUBBLE POPULATIONS

Before the dispersion algorithms (section 2) can be applied to a depth dependent bubble population, a basic knowledge of the variation of bubbles with depth must be sought.

This section presents historical data of bubble populations taken at different depths to allow the reader to apply the results in simulations.

3.1 Bubble Size Distributions in the Ocean

Figure 5 shows a comparison of five historical measurements of the near surface bubble population in deep water and at high wind speed. These studies are specifically, Farmer and Vagle (1989, 1997), Johnson and Cooke (1979), Breitz and Medwin(1989) and Phelps and Leighton (1998). The population density is presented in terms of $n_b(R_0)$, the number of bubbles at a particular bubble radius per cubic meter of water per micrometer radius range.

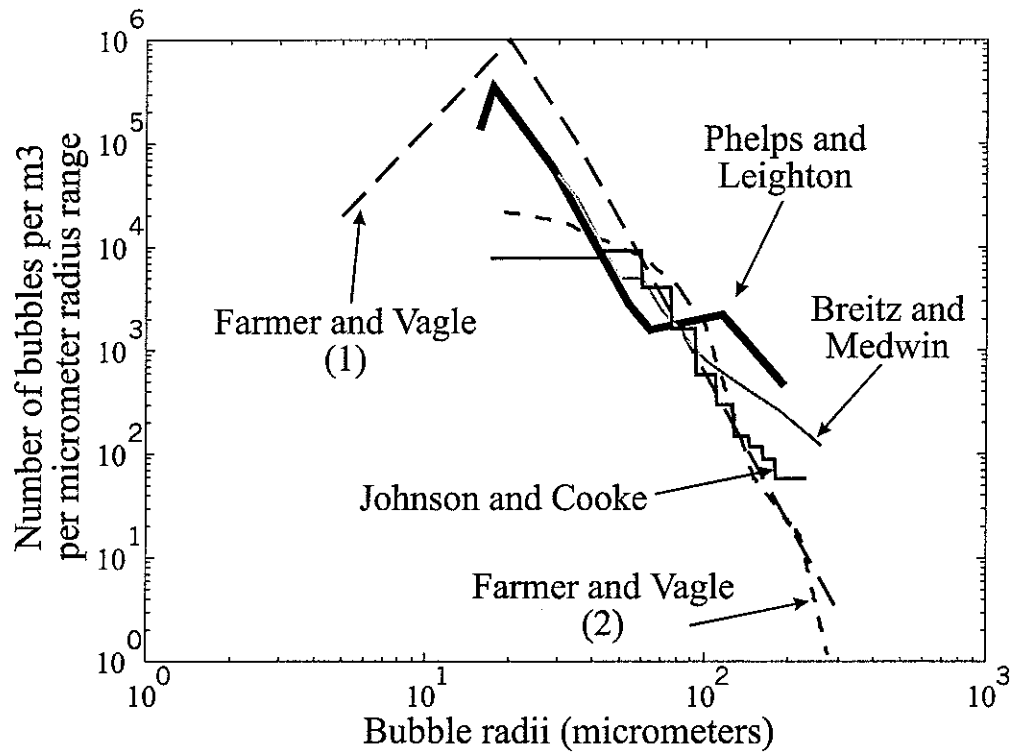

Figure 5: *A comparison of five historical measurements of the near surface bubble population in deep water and at high wind speed. The data is taken from references (Johnson and Cooke, unbroken); (Farmer and Vagle (1) from their 1989 study, large dashes); (Breitz and Medwin, unbroken); (Farmer and Vagle (2) from their 1997 study, small dashes); and (Phelps and Leighton, bold solid line).*

These measurements were all recorded near the surface (<1.5 m) in deep water (using an oceanographic definition) in high wind speeds (11-15 m/s).

The earliest deep water bubble population measurements were performed by Johnson and Cooke who employed a sophisticated optical measurement technique in 20-30 m deep water. Their data for 0.7 m depth and 11-13 m/s wind speed is shown in Fig. 5, compared with other historical measurements which are described below. Their data shows a steady increase in the population between ~ 200 μm and 60 μm, which then flattens out until approximately 20 μm. However, other workers have commented that the photographic observations lack the necessary resolution to observe these smaller bubbles, and that the measured population may underestimate the actual population.

These optical measurements were followed by an acoustic technique of Farmer and Vagle (1989) which used four upwardly facing sonar transducers and monitored the linear backscatter at the four frequencies 28, 50, 88 and 200 kHz. The data was used to infer an ambient bubble population which was then used in modelling the waveguide propagation characteristics in the bubble layer. The population estimates inferred from the strength of the backscattered signal were iteratively matched to the Johnson and Cooke optical data at large bubble size. The estimated population is also shown in Fig. 1, taken at 10 cm depth and in 12-14 m/s wind speed from the Fasinex location, and shows the population to rise up to a maximum at 20 μm of around 1×10^6 bubbles per m^3 per 1 μm radius increment.

The third notable historical measurement was performed by Breitz and Medwin (1989) who used a flat plate resonator to characterise the local oceanic population. This technique again relies on the linear bubble behaviour to affect the attenuation of modes set up between the two resonator plates, which can be used to infer population numbers for bubbles resonant at those modal frequencies. The technique can yield absolute measures of the bubble population, and their measurements are shown on Fig. 5 with the other two historical estimates. This data was collected at 25 cm below the sea surface in 120 m water depth in a 12 m/s wind speed. Their data shows a monotonically increasing bubble population between 250 and 30 μm, but with a higher number of larger bubbles than the other two estimates and a slightly reduced number of smaller bubbles than those estimated by Farmer and Vagle in the same year.

A fourth measurement of the oceanic population is presented again by Farmer and Vagle (this time in 1997), who themselves employed an acoustic resonator, but with a larger radius span than the earlier Breitz and Medwin experiment. Their data was taken at a lower depth of 1.3 m, although in wind speeds comparable with the other data shown (10 m/s). Typical data is shown in Fig. 5 with the other historical measurements. The data shows good agreement with the earlier workers for bubbles larger than 40 μm, and then dips off to fall between the Breitz and Medwin data and that of Johnson and Cooke for smaller bubbles. This may be due to the greater depth at which the recent Farmer and Vagle population was measured, or a limitation of their measurement technique. The workers calibrate their data by using their measured population to calculate the sound speed anomaly due to the presence of the bubbles, and compare this directly with measured sound speed data. The agreement is excellent for larger bubbles, but at the smallest bubble sizes there is a divergence between the measured value and predicted estimate.

The requirement of this section is to obtain simple expressions for the depth dependence of the number of bubbles per cubic metre within one micrometre increment of radius. That is to say, we require of $n_b(R_0,z)$. The first stage will be to express of $n_b(R_0)$ for a fixed depth z, the data given in Figure 1.

Take the Breitz and Medwin data, for example. From resonance broadening measurements for nine specific bubble sizes in the range 30 μm<R_0<270 μm, Breitz and Medwin found an average bubble density of

$$n_b(R_0) = 7.8 \times 10^8 \left[\frac{R_0}{[1\mu m]}\right]^{-2.7}, \text{ (for 30 } \mu\text{m} < R_0 < 270\ \mu\text{m)} \qquad (22)$$

In the same radius range the maximum bubble density detected was $n_b(R_0) = 1.6 \times 10^9$ $[R_0/1\ \mu m]^{-2.7}$. Medwin and Breitz however found that only the larger bubbles in the range 60 μm<R_0<240 μm followed a $n_b(R_0)$ α $[R_0/1\ \mu m]^{-2.6}$ distribution: the population of smaller bubbles (30 μm<R_0<60 μm) decayed as $n_b(R_0)$ α $[R_0/1\ \mu m]^{-4}$. A $[R_0/1\ \mu m]^{-4}$ model distribution fits most of the data obtained by bubble counting reasonably well.

This can be done with the other historical data sets (Figure 6).

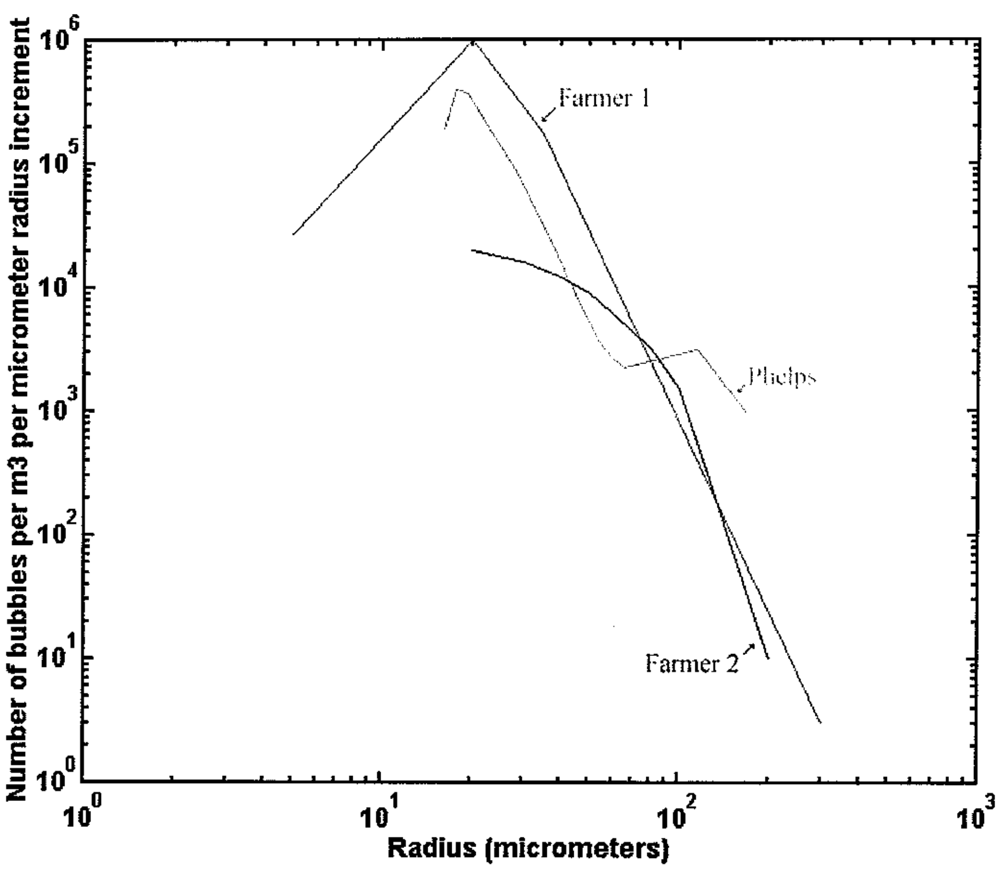

Figure 6: *A comparison of the three historical measurements that require defining as simple expressions. The data is taken from references (Farmer and Vagle (1) published in 1989); (Farmer and Vagle (2) published in 1997); and (Phelps and Leighton, 1998).*

Expressions for each of the bubble distributions shown in figure 6 were determined by curve fitting linear, logarithmic, polynomial, power and exponential functions to the data in a least squares sense. The function that gave the best qualitative fit to the data was selected. The Farmer and Vagle (1989) and Phelps and Leighton (1998)

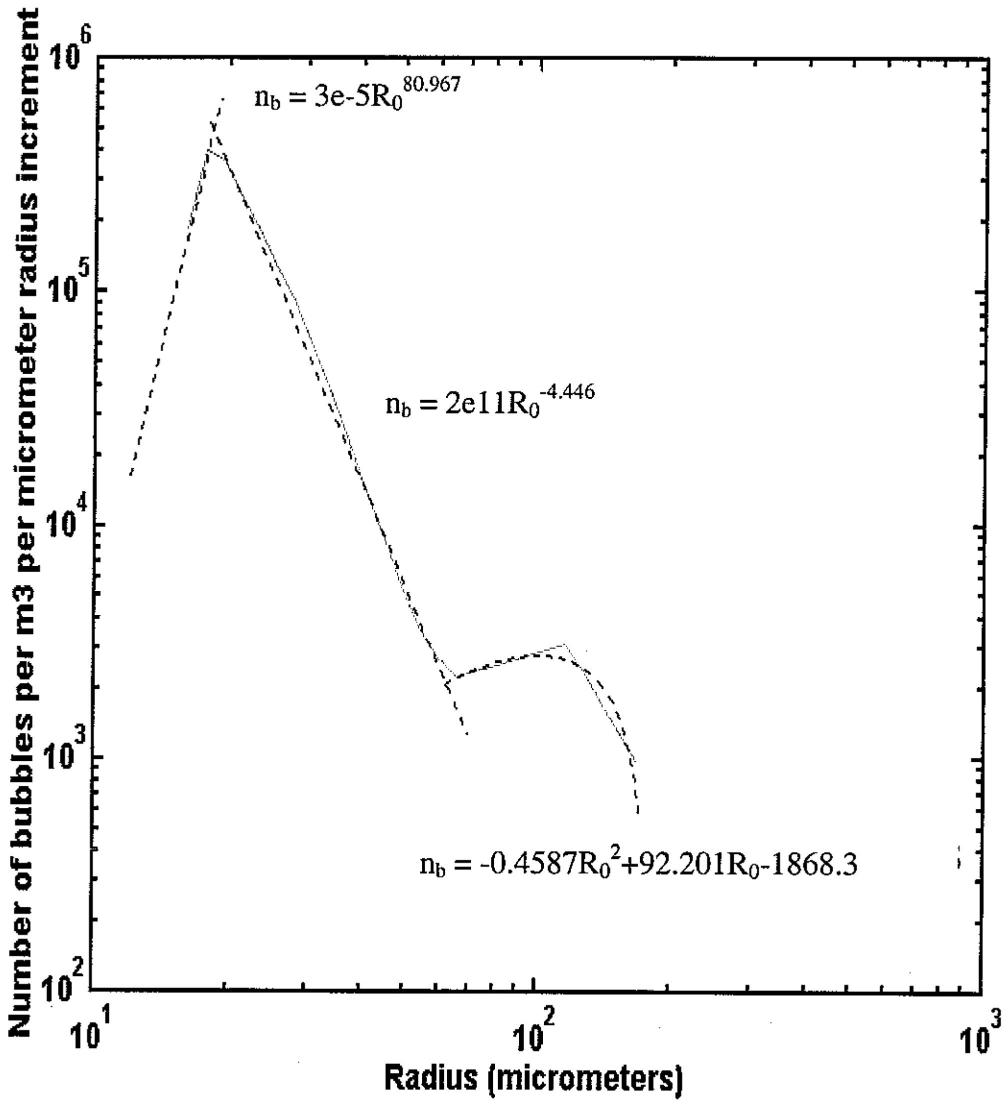

Figure 8: *The Phelps and Leighton data set was defined using two power law equations and a polynomial expression. The power law equation cross at the peak in the distribution and the polynomial expression accounts for the increased large bubbles measured. The resulting distribution (indicated by the dashed line) is overlaid for comparison. The equation for the distribution is also shown were n is the number of bubbles per m^3 per μm radius increment and R is the bubble radius in μm.*

The Phelps and Leighton (1998) population was estimated using two power law functions and a polynomial function to account for the increased number of large bubbles measured (figure 8). The first equation (25) is valid up to 18 μm and the second equation (26) is valid from 19 μm to 62 μm. The final equation (27) is valid from 63 μm to approximately 170 μm. Owing to the nature of the polynomial expression this rapidly tends to zero for bubble radii > 170 μm.

populations were modelled in this fashion but using a series of expressions to obtain a good fit to the data.

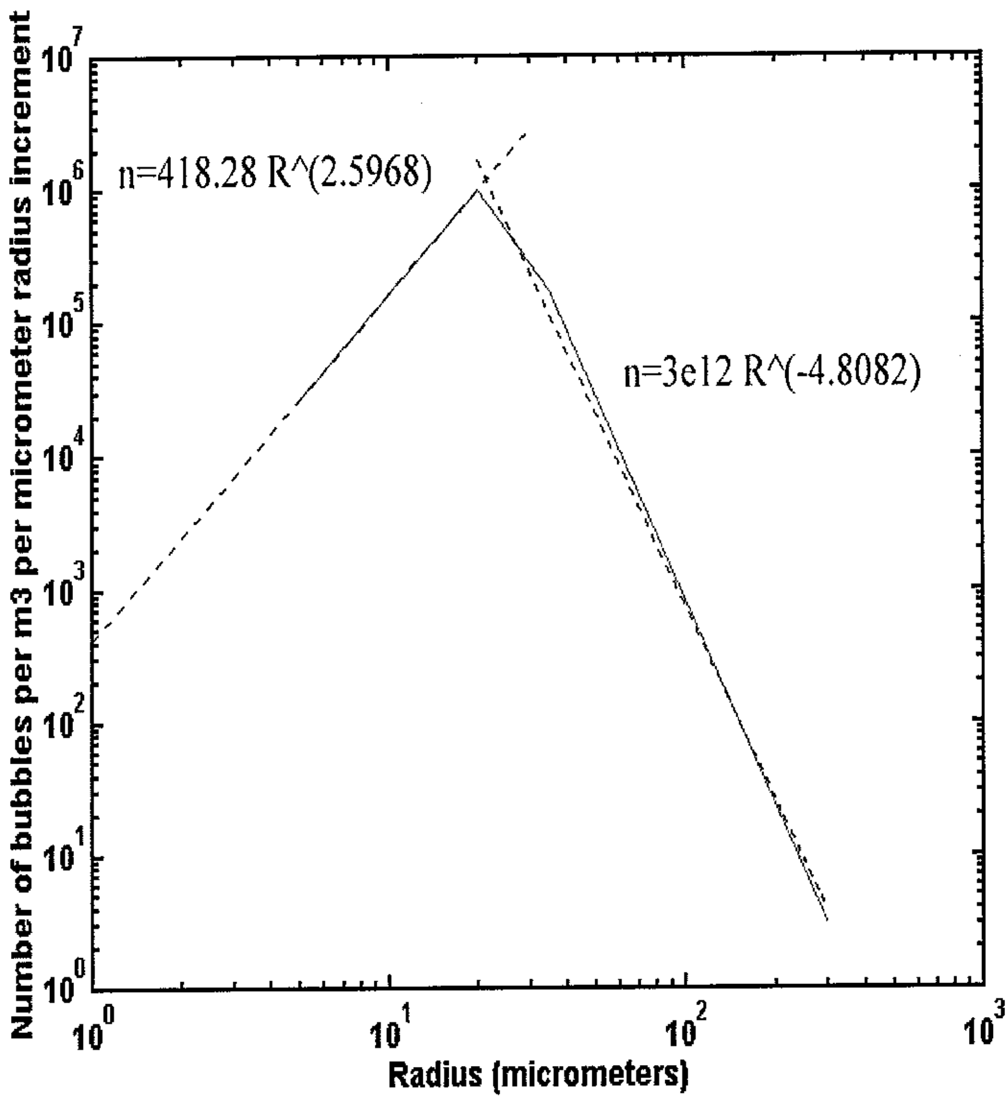

Figure 7: *The Farmer and Vagle (1989) data set was defined using two power law equations crossing at the peak in the distribution. The resulting distribution (indicated by the dashed line) is overlaid for comparison. The equation for the distribution is also shown where n_b is the number of bubbles per m^3 per μm radius increment and R is the bubble radius in μm.*

The 1989 Farmer and Vagle (1) population was estimated using two power law functions (figure 7). The first equation (23) is valid up to 21 μm and the second equation (24) is valid from 22 μm.

$$n_b(R_0) = 418.28\frac{R_0^{2.5968}}{1\mu m} \tag{23}$$

$$n_b(R_0) = 3e12\frac{R_0^{-4.8082}}{1\mu m} \tag{24}$$

$$n_b(R_0) = 3e-5\frac{R_0^{8.0967}}{1\mu m} \tag{25}$$

$$n_b(R_0) = 2e11\frac{R_0^{-4.446}}{1\mu m} \tag{26}$$

$$n_b(R_0) = -0.4587\frac{R_0^2}{1\mu m} + 92.201\frac{R_0}{1\mu m} - 1868.3 \tag{27}$$

The final distribution, that of Farmer and Vagle 1997 (2), is approximated using a single exponential expression given in equation (28).

$$n_b(R_0) = 6941e^{-0.0426\frac{R_0}{1\mu m}} \tag{28}$$

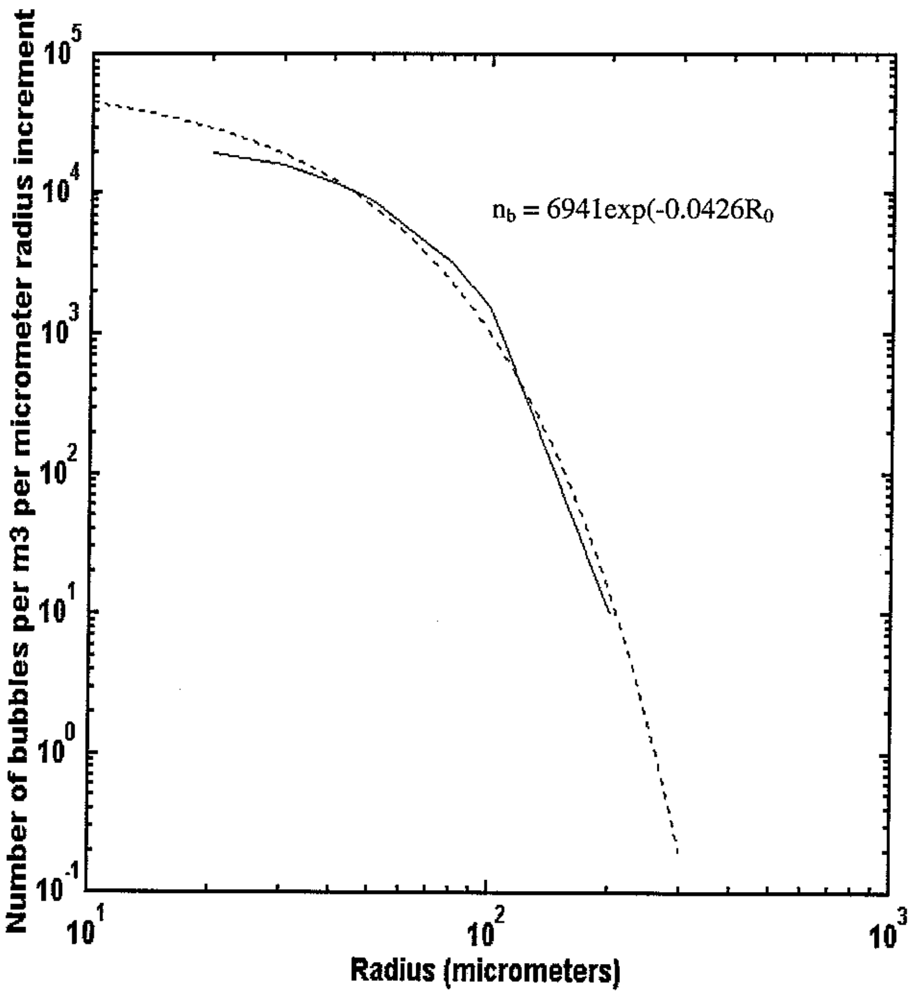

Figure 9: *The 1997 Farmer and Vagle (2) data set was defined using an exponential expression. The resulting distribution (indicated by the dashed line) is overlaid for comparison. The equation for the distribution is also shown where n_b is the number of bubbles per m^3 per μm radius increment and R is the bubble radius in μm.*

3.2 Bubble e-folding Depth

Once an expression has been obtained for the bubble size distribution at a specific depth (see previous section), the requirement is to produce a depth-dependent expression for the bubble population distribution. Vertical arrays of bubble sensors have been deployed, but searches have not yielded any published reports of the depth-dependence of the bubble population from this trial[2]. However an estimate population can be found by combining the fixed-depth populations calculated above, noting the depth at which each was taken, and fitting to them an e-folding depth (of course, variations in windspeed and water depth will reduce the validity of combining such data in this manner, but the technique is sufficient for this estimation).

The population measurements of Farmer and Vagle (1989), Phelps and Leighton (1998) and Farmer and Vagle (1997) were taken at a depth of 0.1 m, 0.5 m, and 1.3 m respectively. The numbers of 20 μm and 30 μm bubbles in each of this distributions can be plotted against depth and an exponential curve of the form $y = ae^{bx}$, where a and b are constants, can be fitted to the data. The resulting average e-folding depth is given by the value of b is 3.3 m and 2.3 m respectively.

These depths are not far from the e-folding depths of backscatter (as opposed to bubble densities) to be found in the literature. Direct sonar measurements in Loch Ness by Thorpe (1982), and his analysis of Johnson and Cooke's sea results, suggest that the acoustic scattering cross-section decays approximately exponentially with depth (with an e-folding depth of metre order), and increases with windspeed. Monahan and Lu characterise β plumes as having decay depths of around 0.5 m. Of course the stronger the effects of turbulence and Langmuir circulation, the greater the depth in general to which the bubble clouds will penetrate, and hence the less the e-folding depth. It is generally accepted that when the circulation is strong the bubble layer can extend to some 10 m below the sea surface.

Direct measurements of bubble size distributions near the ocean surface were acquired in the Gulf of Mexico using acoustic resonators (Farmer *et al.*, 1998). The data were collected at five different depths with the wind speed ranging from 7.5 to 15 m/s. There is much temporal variability in the results, but when averaged, the size distribution the data appear to fit the following empirical relation:

$$n_b(R_0, z, W) = BW^p \exp(-z/D) p(R_0), \tag{29}$$

with

$$p(R_0) = \begin{cases} R_0^{-p_1} & R_0 \le a_0 \\ \beta R_0^{-p_2} & R_0 > a_0 \end{cases}, \tag{30}$$

where W is wind speed at 10m, and z is depth below the instantaneous ocean surface. Farmer found that $a_0 = 100\ \mu$m was appropriate for the data set, with $p_1 \sim -1.75$ and p_2

[2] However a personal approach by Prof. Leighton to Prof. Farmer of produced some unpublished data which is discussed at the end of this section.

~ 5.0. The parameter $\beta = a_0^{(p_2-p_1)} = a_0^{6.75}$ is adjusted to ensure continuity at a_o and B = 4094. It should be emphasised that this is a simplification. For example there is some evidence that a_o decreases somewhat with depth and this is not included. There is also systematic evolution of the bubble size spectrum with time following injection by the breaking wave. The e-folding depth found by Farmer was D_e = 0.7 m.

3.3 Inclusion of Depth Dependence into Calculations for Dispersion in Bubbly Media

The continuous depth dependence of a bubble population can be written discretely in terms of flat splines that interpolate the bubble population for a particular radii with respect to depths z_J to z_{J+1}.

$$n_b(R_0, z) = \sum_{J=1}^{N} n_{bJ}(R_0) \tag{31}$$

This equation descretises the continuous depth dependent bubble distribution $n_b(R_0,z)$ into a series of linear and flat equations that describe the bubble distribution function over the depth domain $[z_J{:}z_{J+1}]$. This is represented in figure 10.

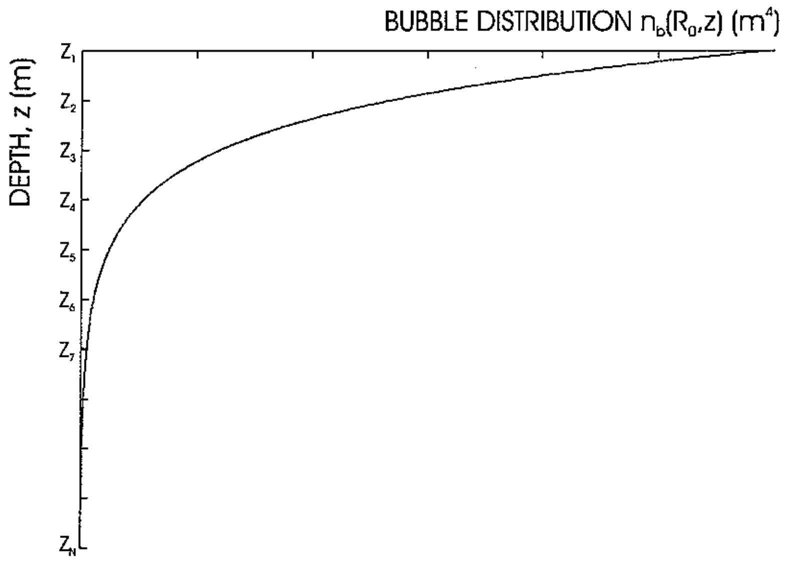

Figure 10: *A continuous bubble distribution function as a function of depth (z). The plot shows the exponential decay of the bubble population for a particular radius R_0 with depth, z. The range of depth is from z_1 to z_N.*

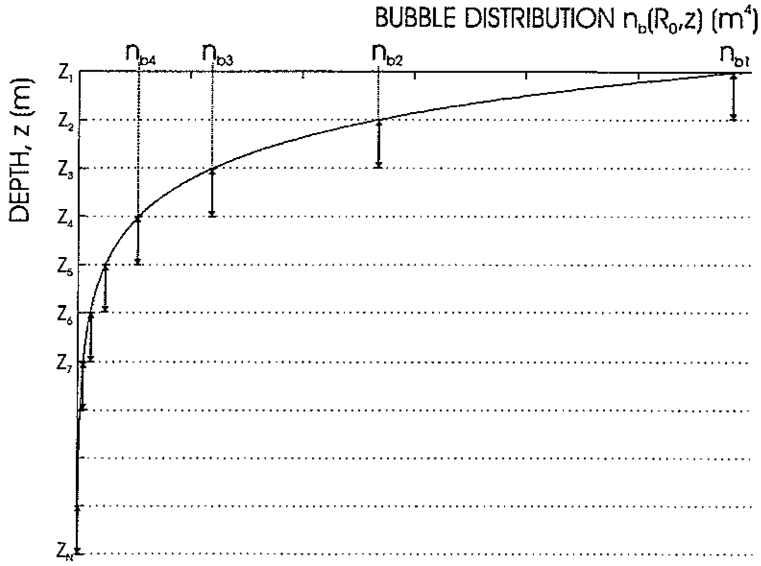

Figure 11: *The descretised representation of the continuous bubble population of Figure 10. The continuous function is represented as a series of linear and flat distributions within the depth domain* $[z_J;z_{J+1}]$

The discretisation of the bubble population as shown in figure 11 allows the dispersive effect of the depth dependant bubble population to be calculated over a finite distance of acoustic propagation. This approach also lends itself to a stratified model of the ocean that may be used in a ray tracing model.

Substitution of equation (31) into equation (18) gives the following depth dependant phase speed ratio.

$$\frac{c^2(z)}{c_m^2(z)} = 1 + 4\pi c^2(z) \int_{R_0=0}^{\infty} \frac{R_0 n_b(R_0,z)}{\omega_o^2(R_0,z) - \omega^2 + 2jb(R_0,z)\omega} dR_0 \tag{32}$$

4.0 CONCLUSIONS

The following section will summarise the equations that are depth dependent and have to be modified from their original form in order that they can be employed in a ray-tracing model.

The first is the depth dependent dispersion ratio which produces phase speed variations and excess attenuation coefficients via equations (20) and (21) respectively.

$$\frac{c^2(z)}{c_m^2(z)} = 1 + 4\pi c^2(z) \int_{R_0=0}^{\infty} \frac{R_0 n_b(R_0,z)}{\omega_o^2(R_0,z) - \omega^2 + 2jb(R_0,z)\omega} dR_0 \tag{33}$$

Equation (31) requires the descretised depth dependent bubble population,

$$n_b(R_0,z) = \sum_{J=1}^{N} n_{b_J}(R_0) \tag{34}$$

resonant frequency of a bubble,

$$\omega_0(z)=\frac{1}{2\pi R_0\sqrt{\rho}}\sqrt{3\kappa\left(p_0(z)+\frac{2\sigma}{R_0}\right)-\frac{2\sigma}{R_0}-\frac{4\mu^2}{\rho R_0{}^2}} \tag{35}$$

damping constant,

$$b(z)=\frac{2\mu}{\rho R_0{}^2}+\frac{p_0(z)}{2\rho R_0{}^2\omega}\Im\Phi+\frac{\omega^2 R_0}{2c} \tag{36}$$

and sound speed,

$$c(z)=1449.2+4.6T-0.055T^2+0.00029T^3+(1.34-0.010T)(S_{ppt}-35)+1.58\times10^{-6}P_o(z) \tag{37}$$

where,

$$P_o(z)=\rho_s g z \tag{38}$$

The depth dependent homogenous attenuation coefficient for saline water can be given as,

$$\alpha_s(z)=\frac{1.71\times10^8(4\mu_f/3+\mu'_f)F^2}{\rho_f c_f^3(z)}+\left(\frac{S_{ppt}A'F_{rm}F^2}{F^2+F_{rm}^2}\right)\left(1-1.23\times10^{-3}P_o(z)\right)+\left(\frac{A''F_{rb}F^2}{F^2+F_{rb}^2}\right) \tag{39}$$

5.0 REFERENCES

Breitz N. and Medwin H., (1989) Instrumentation for in situ acoustical measurements of bubble spectra under breaking waves. *J. Acoust. Soc. Am.*, **86**, 739-743, 1989.

Clay C.S. and Medwin H., (1977). Acoustical Oceanography: Principles and Applications. *John Wiley and Sons.*

Commander K.W. and Prosperetti A., (1989) Linear pressure waves in bubbly liquids: comparison between theory and experiments. *J. Acoust. Soc. Am.*, **85**, 732-746.

Farmer D.M. and Vagle S., (1989) Waveguide propagation of ambient sound in the ocean-surface bubble layer. *J. Acoust. Soc. Am.*, **86**, 1897-1908.

Farmer D.M. and Vagle S., (1997) Bubble measurements using a resonator system, in *Natural physical processes associated with sea surface sound*, T.G. Leighton, Ed. Institute of Sound and Vibration Research: University of Southampton, 155-162.

Johnson B.D. and Cooke R.C., (1979) Bubble populations and spectra in coastal waters: a photographic approach. *J. Geophys. Res.*; **84**, C7: 3761-3766.

Leighton T.G., (1994) *The Acoustic Bubble,* Academic Press, London.

Leighton, T.G., Phelps, A.D., Simpson, M.D., (January 1998) Oceanic Bubble Sizing: Measurements and Proposed Studies. *ISVR Technical Report No. 273.*

Medwin H., Breitz N.D., (1989) Ambient and transient bubble spectral densities in quiescent seas and under spilling breakers. *J. Geophys Res.* **94**, 12751-12759.

Monahan E.C. and Lu N.Q., (1990) Acoustically relevant bubble assemblages and their dependence on meteorological parameters. *IEEE J. Oceanic Eng.* **15**, 340-345.

Phelps A.D. and Leighton T.G., (1997) Measurement of bubble populations near the sea surface using combination frequencies: adaptation and calibration of device between two sea trials, in *Natural physical processes associated with sea surface sound*, T.G. Leighton, Ed. Institute of Sound and Vibration Research; University of Southampton, 198-210.

Phelps A.D. and Leighton T.G., (1998) Oceanic bubble population measurements using a buoy-deployed combination frequency technique. *IEEE Journal of Oceanic Engineering*, **23**(4), 400-410.

Thorpe S., On the clouds of bubbles formed by breaking wind-waves in deep water, and their role in air-sea gas transfer. *Philos. Trans. R Soc* London 1982; A304: 155-210

Walsh A.L. and Mulhearn P.J., (1987) Photographic measurements of bubble populations from breaking waves at sea. *J. Geophys. Res.*, **92**(C13), 14553-14565.

Woolf D.K. and Thorpe S.A. (1991) Bubbles and the air-sea exchange of gases in near-saturation conditions. *J. Marine Res.* **49,** 435-466.